Electronic Supplementary Material (ESI) for CrystEngComm.

Supporting Information

Carbon dioxide induced structural phase transition in metal-organic frameworks CPO-27

Breogán Pato-Doldán,[a] Mali H. Rosnes,[a] Dmitry Chernyshov[b] and Pascal D. C. Dietzel[a]*

[a] Department of Chemistry, University of Bergen, P.O. Box 7803,
N-5020 Bergen, Norway. E-mail: pascal.dietzel@uib.no
[b] Swiss–Norwegian Beamlines at the European Synchrotron Radiation Facility,
38000 Grenoble, France.

Experimental Details

Materials

CPO-27-M (M = Co and Zn) materials were synthesized under solvothermal conditions according to experiment procedures in ref. 1 and CPO-27-Ni using the procedure in ref. 2. All chemicals, reagents and solvents were purchased from Sigma-Aldrich and used as received without further purification. Purity of the products was confirmed by powder X-ray diffraction. Solvent was removed by pre-treating the samples at 453 K (Zn) and 423 K (Co, Ni) for 24 hours under dynamic vacuum. The textural properties of the samples were confirmed via N_2 adsorption measurements at 77.36 K. The guest-free powder samples were stored in a glovebox under argon atmosphere and filled into glass capillaries (ø=0.5 mm). Afterwards each capillary was sealed.

Volumetric gas adsorption

Volumetric gas adsorption measurements were carried out on a BELSORP-max instrument equipped with a low pressure transducer and a turbomolecular pump, allowing highly precise measurements from very low pressures (p/p_0 = 10^{-8}). The gases used for gas adsorption measurements were of 99.9995% or higher purity and were purchased from Yara Praxair.

Sample	BET specific surface area / $m^2\ g^{-1}$	Langmuir specific surface area / $m^2\ g^{-1}$	Pore volume (at p/p_0 = 0.500)
CPO-27-Co	1276	1362	0.48
CPO-27-Zn	1187	1274	0.45
CPO-27-Ni	1331	1446	0.53

Variable temperature synchrotron powder X-ray diffraction

Powder X-ray diffraction experiments were carried out at the Swiss–Norwegian Beamlines (BM01) at the European Synchrotron Radiation Facility (ESRF). A modified capillary sample holder, available at SNBL, was used for these experiments.[3] The sample capillary was opened on one end to permit connection to vacuum and gas dosing and the sample holder was connected to a custom built gas dosing system which allowed evacuation of the sample or exposure to a static pressure of CO_2.[4] Quartz-glass fibers were placed on one side of the sample within the capillary to reduce the risk of the sample moving within the capillary as pressure changes were applied during the experiment.

An Oxford Cryostream 700 system was placed close to the capillary in such a way that the cooling (or heating) zone covered the X-ray beam width. The samples were heated in vacuo at 453 K before the CO_2 adsorption experiment. Data of the activated samples were then recorded and analyzed immediately in order to assure the complete removal of any adsorbed guest molecule before progressing with the CO_2 adsorption experiment. The activated sample was afterwards exposed to 1 bar of CO_2 pressure. Outside of the cooling zone of the Cryostream, the rest of the capillary and gas supply line is at room temperature, thus maintaining the pressure at the sample during the temperature program. Data were collected using a DECTRIS PILATUS 2M area detector. A wavelength of 0.69570 Å, a sample to detector distance of 446 mm, and an exposure time of 20 seconds were used. The azimuthal integration of raw images was performed with the program Bubble.[5] Profile fits and Rietveld refinements of the powder diffraction patterns were performed using TOPAS 6.[6] The occurrence of solid CO_2 in diffraction patterns due to condensation below

195 K was accounted for by adding a second non-structural phase in the profile fits and Rietveld refinements.

The crystal structure of CPO-27-Co loaded with CO_2 at 1 bar at 97.2 K was solved by simulated annealing and subsequently refined using the Rietveld method. A Chebyshev function of eight terms was used to fit the background and a broad Pseudo-Voigt peak was used to account for the contribution of the capillary to the background. 28 soft distance restraints and 40 angle restrains were applied to maintain the connectivity of the atoms of the two 2,5-dioxidoterephthalate linkers. Rigid bodies were employed to account for the CO_2 molecules inside the CPO-27-Co framework cavities. The C–O bond length in the CO_2 molecules was restrained in the range 1.1-1.2 Å and the C–O–C angle was constrained to 180°. The modeled atoms within each CO_2 molecules were constrained to maintain the same fractional occupancies throughout the refinement. Isotropic displacement parameters were used for all the atoms in the structure.

The LT phase has only a few additional reflections with weak intensity in comparison to the HT phase, but a significant increase in atomic parameters. One consequently has to expect that the structure determination, and in particular the positions, site occupancy factors and thermal parameters of the CO_2 guest molecules are less accurate for the LT phase than for the HT phase. This is reflected, for instance, by the variation of Co–O(CO_2) distances, which are in the range 2.3(1)-2.7(1) Å in the LT phase (compared to 2.37(2) Å in the HT phase). Nevertheless, the structure refinement clearly shows how the framework atoms re-arrange in the LT phase.

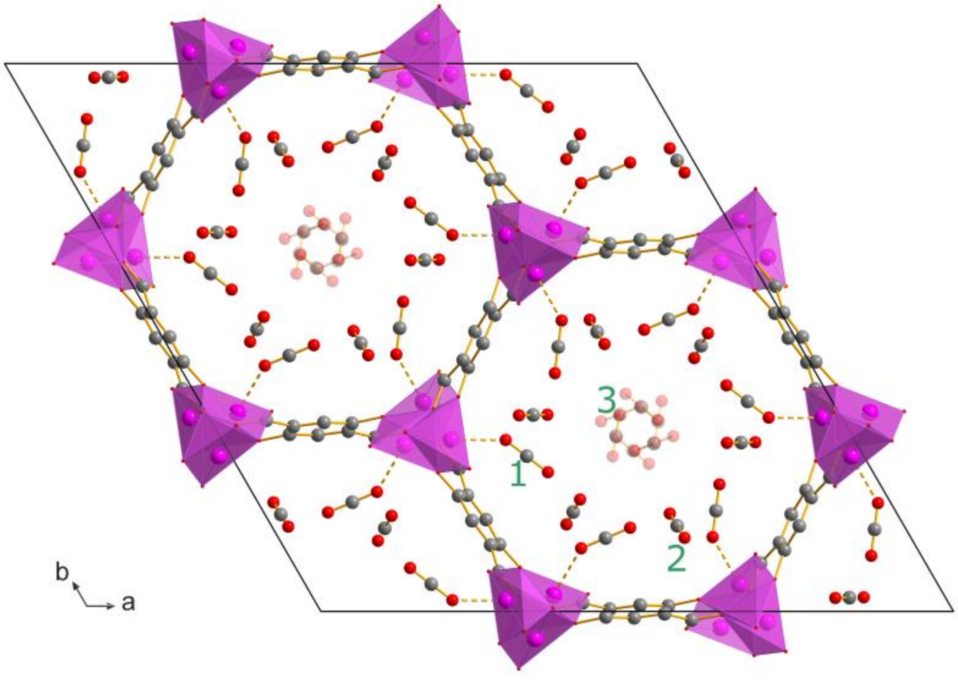

Figure S1. View along the channels of the CPO-27-Co structure at 120 K and 1 bar CO_2, showing the three adsorption sites. C atoms are drawn in gray, O in red, and Co in magenta.

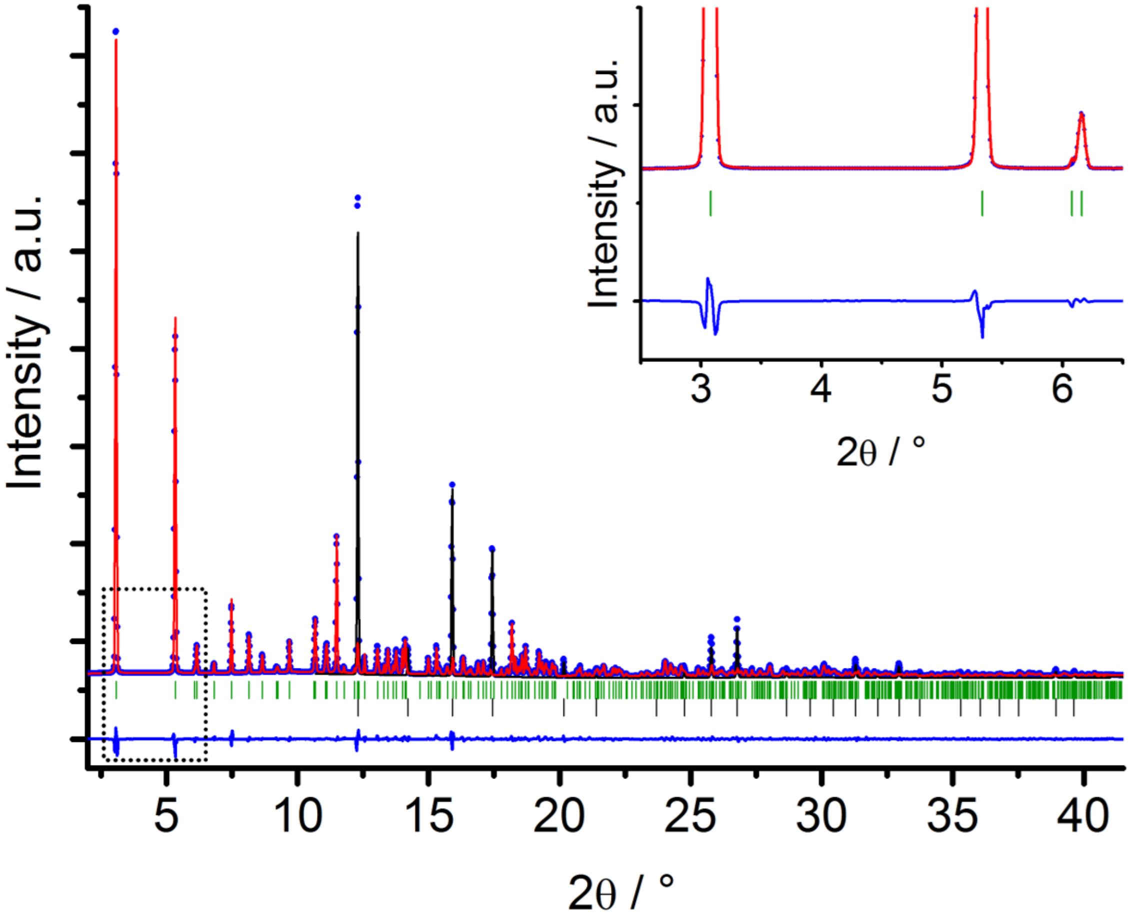

Figure S2. Rietveld refinement plot of synchrotron (λ= 0.6957 Å) powder X-Ray diffraction data of CPO-27-Co measured at 120 K and 1 bar CO_2. Blue points represent the experimental diffraction pattern, the red line represents the calculated pattern of CO_2 loaded CPO-27-Co and the black line the calculated pattern of solid CO_2. The blue line at the bottom represents the difference between experimental and calculated patterns, while the green and black tick marks represent the Bragg reflections for the CPO-27-Co and solid CO_2 phases, respectively. Inset: zoom into the 2.5-6.5° 2θ range.

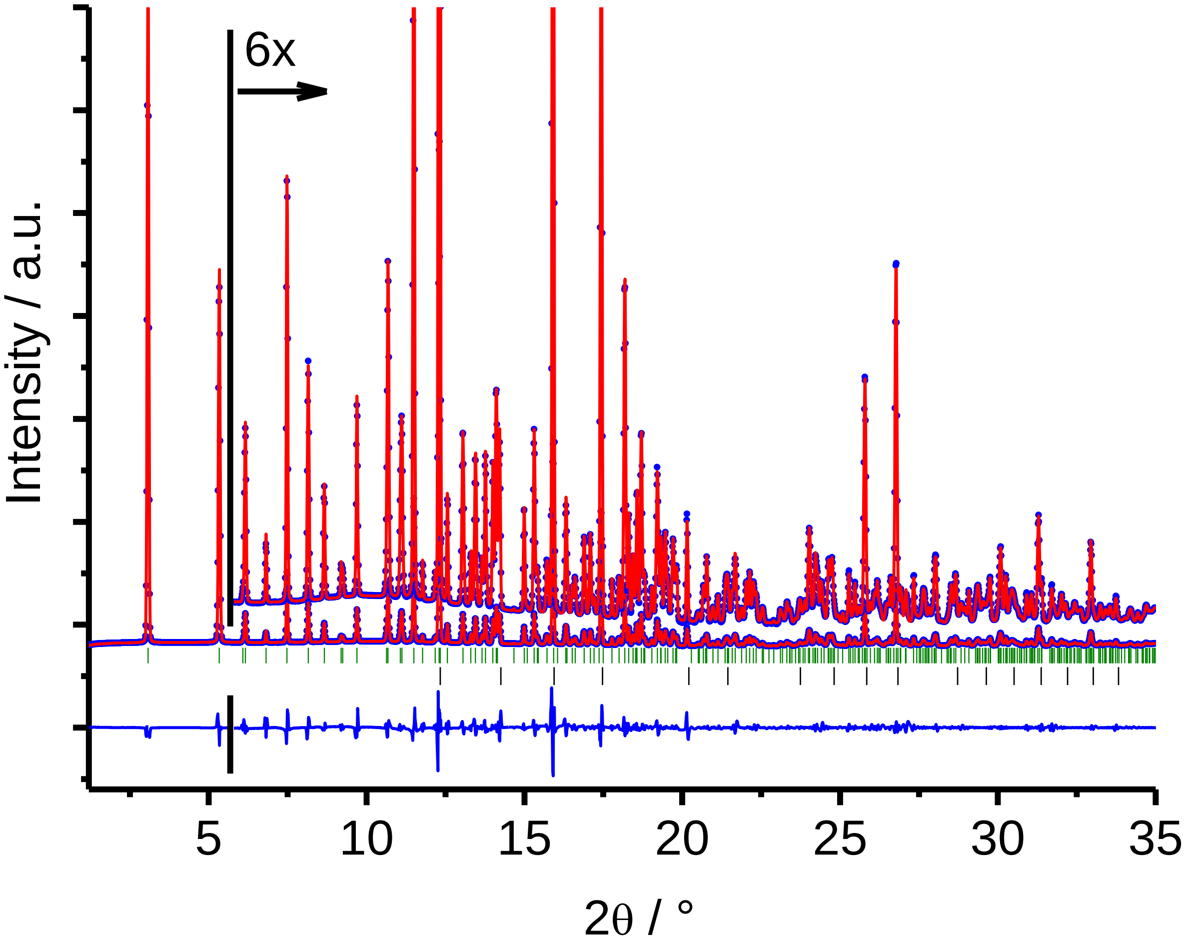

Figure S3. Pawley fit of synchrotron (λ= 0.6957 Å) powder X-Ray diffraction data of CPO-27-Co measured at 112 K and 1 bar CO_2. Blue points represent the experimental diffraction pattern, while the red line represent the calculated pattern of CO_2 loaded CPO-27-Co and solid CO_2. The blue line at the bottom represents the difference between experimental and calculated patterns, while the green and black tick marks represent the Bragg reflections for the CPO-27-Co and solid CO_2 phases, respectively.

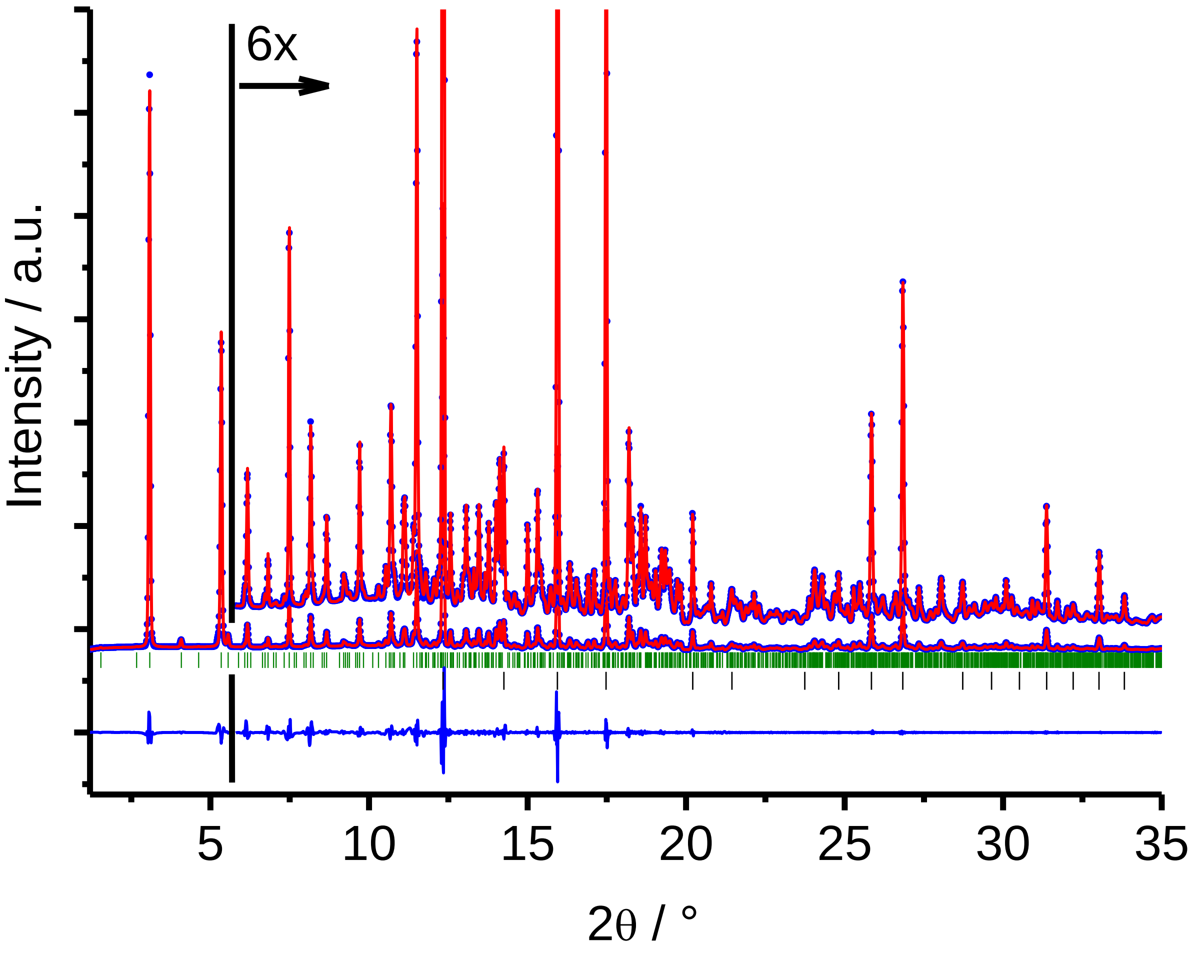

Figure S4. Pawley fit of synchrotron (λ= 0.6957 Å) powder X-Ray diffraction data of CPO-27-Co measured at 97 K and 1 bar CO_2. Blue points represent the experimental diffraction pattern, while the red line represent the calculated pattern for CO_2 loaded CPO-27-Co and solid CO_2. The blue line at the bottom represents the difference between experimental and calculated patterns, while the green and black tick marks represent the Bragg reflections for the CPO-27-Co and solid CO_2 phases, respectively.

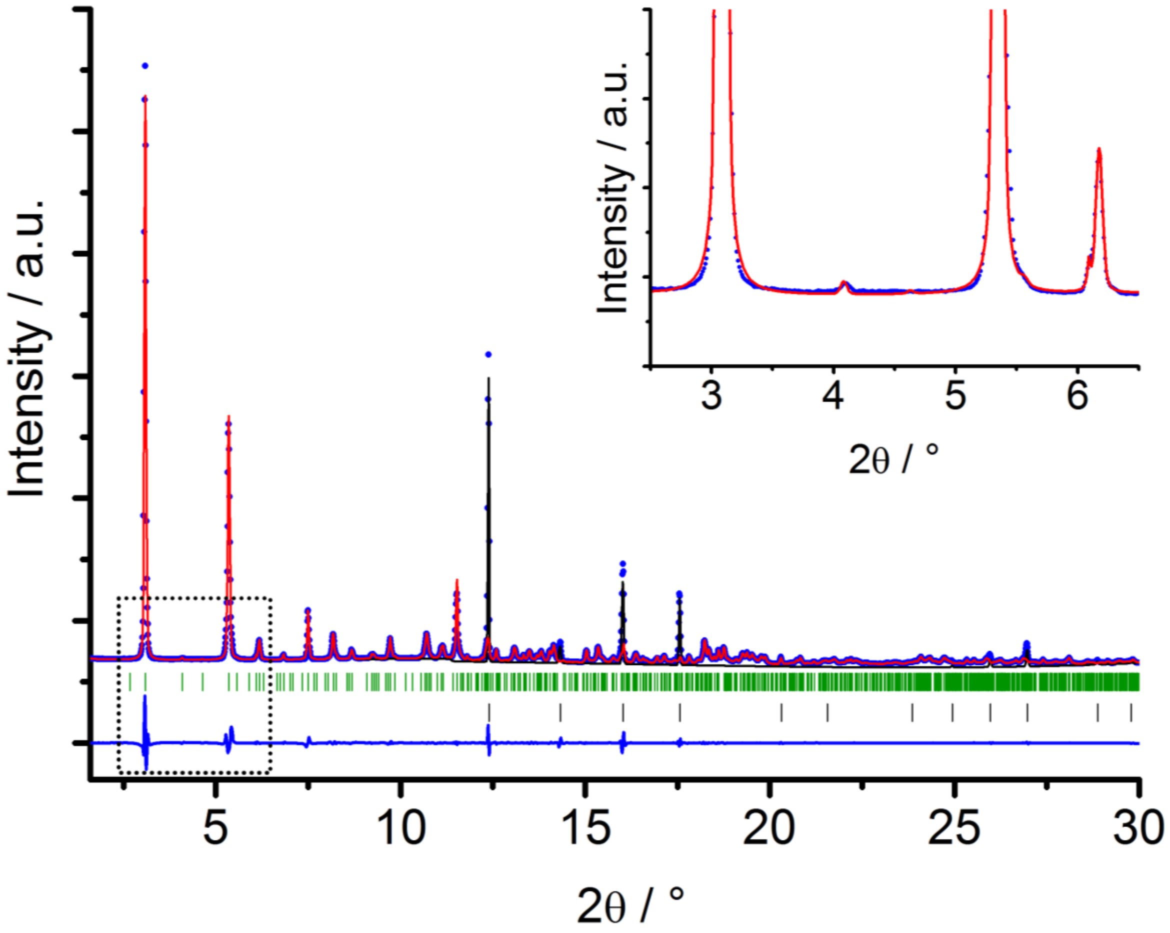

Figure S5. Pawley fit of synchrotron (λ= 0.6957 Å) powder X-Ray diffraction data of CPO-27-Zn measured at 97 K and 1 bar CO_2. Blue points represent the experimental diffraction pattern, the red line represents the calculated pattern of CO_2 loaded CPO-27-Zn and the black line the calculated pattern of solid CO_2. The blue line at the bottom represents the difference between experimental and calculated patterns, while the green and black tick marks represent the Bragg reflections for the CPO-27-Zn and solid CO_2 phases, respectively. Inset: zoom into the 2.5-6.5° 2θ range.

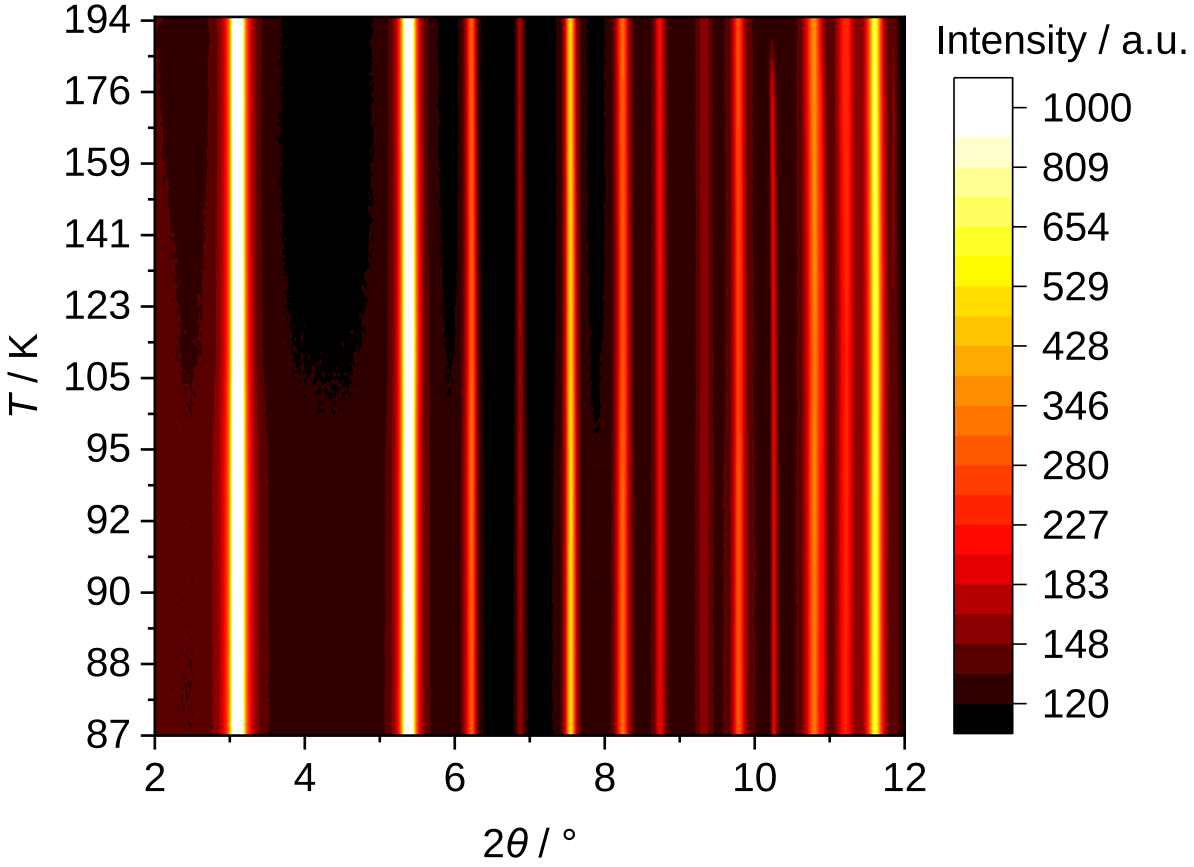

Figure S6. Evolution of the variable temperature powder X-ray diffraction patterns of CPO-27-Ni in CO_2 atmosphere (1 bar) upon cooling from 195-87 K (λ = 0.69730 Å).

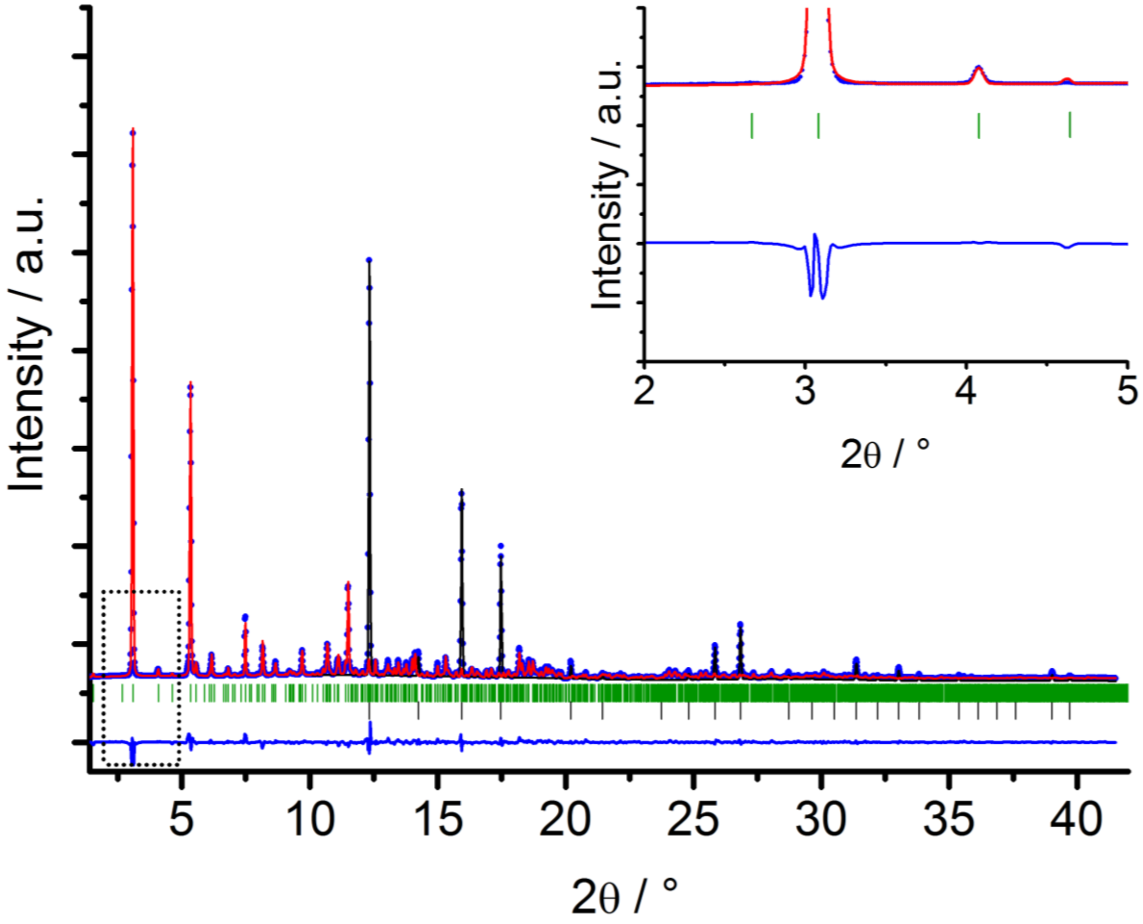

Figure S7. Rietveld refinement plot of synchrotron (λ= 0.6957 Å) powder X-Ray diffraction data of CPO-27-Co measured at 97 K and 1 bar CO_2. Blue points represent the experimental diffraction pattern, the red line represents the calculated pattern of CO_2 loaded CPO-27-Co and the black line the calculated pattern of solid CO_2. The blue line at the bottom represents the difference between experimental and calculated patterns, while the green and black tick marks represent the Bragg reflections for CPO-27-Co and CO_2, respectively. Inset: zoom into the 2-5° 2θ range.

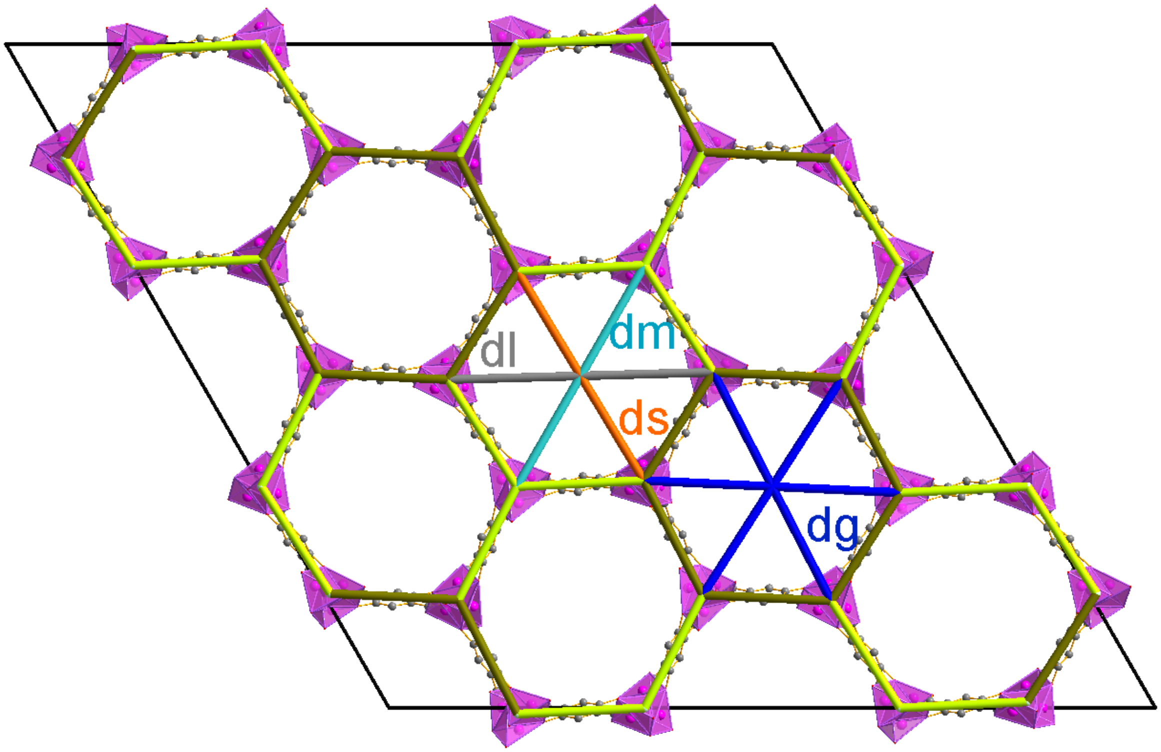

Figure S8. View of the CPO-27-Co LT phase structure along [001]. The principal diagonals of the hexagonal cavities have been estimated by measuring the distance between the center of mass of the SBUs located in diametrically opposite vertices of the hexagon: dg (17.41 Å), dl (17.95 Å), dm (17.28 Å) and ds (16.52 Å). C atoms are reported in gray, O in red, and Co in magenta. H atoms and CO_2 molecules are omitted for clarity.

Table S1. Crystallographic data for the Rietveld refinements of the CO_2 loaded CPO-27-Co at 120 K and 97 K.

CPO-27-Co	**HT**	**LT**
Refinement Method	Rietveld	Rietveld
T / K	120	97
$p(CO_2)$ / bar	1	1
Space group	$R\overline{3}$	$R\overline{3}$
Z	18	72
a / Å	25.8879(4)	51.851(2)
c / Å	6.8586(1)	6.8749(3)
V / Å^3	3980.7(1)	16007(1)
λ / Å	0.6973	0.6973
2θ range / °	2-41	1.4-40
R_p	3.673 %	5.451 %
R_{wp}	5.524 %	7.088 %
R_{exp}[a]	0.02208 %	0.022 %
R_{Bragg}	2.093 %	4.248 %
GoF[a]	250.1	321.3

[a] GoF values are calculated from the expected and weighted profile R factors using the following expression: GoF = R_{wp}/R_{exp}. High GoF values can occur if data are collected to very high precision, in these cases, minor imperfections in the fit become huge with respect to the experimental uncertainty. Under these circumstances R_{exp} is very small and the GoF value is large, for example see refs. 7 and 8.

Table S2. Comparison of selected bond distances and angles for the crystal structure of CO_2 loaded CPO-27-Co structures at 120 K and 97 K. Note that the positions and distances in the LT phase, and in particular those involving the CO_2 guest molecules, must be considered to be less accurate than implied by the standard deviations due to difficulty in obtaining precise positions, site occupancy factors and thermal parameters of the CO_2 molecules in the structure refinement of the LT phase.

Bond distance / Å	**HT**	**LT**			
	Co	**Co1A**	**Co1B**	**Co1C**	**Co1D**
M-O(carboxylate)	2.08(1)	2.15(4)	2.20(4)	2.42(4)	2.20(3)
	2.04(2)	2.08(6)	2.12(4)	2.04(5)	2.17(5)
	2.01(1)	2.06(5)	2.08(4)	1.94(3)	2.07(6)
M–O(oxido)	2.00(1)	2.02(4)	2.06(4)	2.17(4)	2.12(5)
	1.99(1)	1.96(3)	1.94(5)	1.86(3)	1.89(5)
M–O(CO_2)	2.37(2)	2.5(1)	2.4(1)	2.68(9)	2.3(1)

Bond angle / °	**HT**	**LT**			
	Co	**Co1A**	**Co1B**	**Co1C**	**Co1D**
O(oxido)–M–O(carboxylate, chelating)	82.6(5)	75(1)	74(2)	70(2)	75(2)
O(oxido)–M–O(carboxylate, non chelating)	101.3(5)	106(2)	109(2)	111(2)	104(2)
	96.5(5)	100(2)	98(2)	106(2)	102(2)
	95.3(5)	99(2)	95(2)	92(2)	93(2)
	80.6(5)	84(2)	84(2)	88(2)	82(2)
	79.6(5)	80(2)	78(2)	72(1)	79(2)
O(carboxylate)–M–O(carboxylate)	96.9(5)	98(2)	99(2)	106(2)	92(2)
	82.3(5)	82(2)	83(2)	80(2)	82(1)
O(CO_2)–M–O(carboxylate)	95.6(6)	95(2)	92(3)	93(2)	98(4)
	85.1(6)	84(3)	85(3)	82(2)	88(4)
O(CO_2)–M–O(oxido)	93.1(6)	90(2)	91(3)	90(2)	95(4)
	90.3(6)	86(2)	87(3)	85(2)	90(4)
M–O–C(CO_2)	146(2)	160(7)	152(9)	162(9)	116(11)

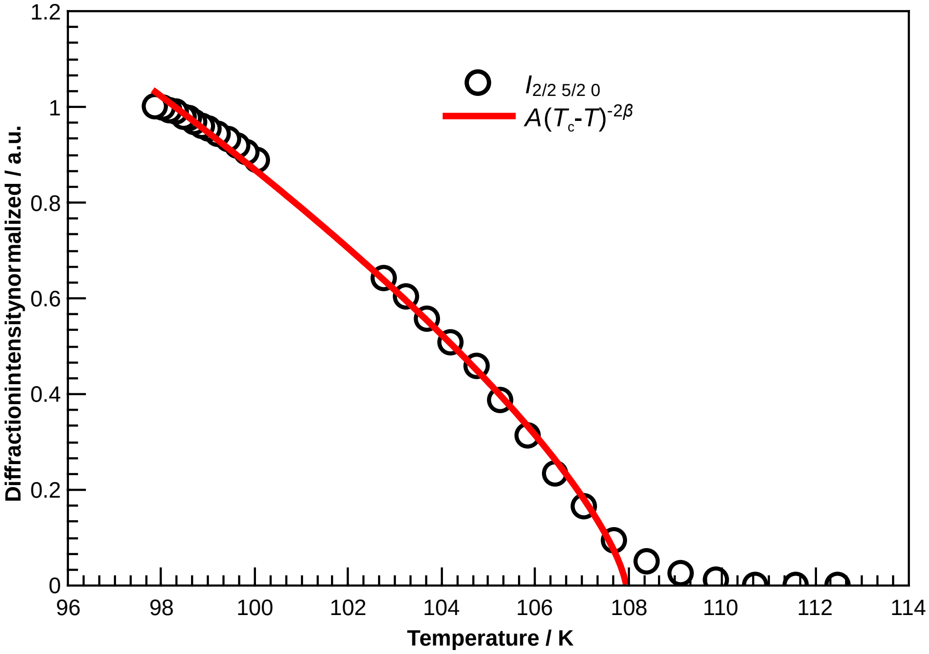

Figure S9. Temperature dependence of diffraction intensity for the [2/2 5/2 0] Bragg line (circles). (Miller indices are given for the HT unit cell.) Red line shows the fit with a critical curve; fitted values are 0.36(2) for the critical index β and 107.9(1) K for the transition temperature T_c. The value of β and gradual increase of intensity on cooling indicates a second order of the transition.

References

1. B. Pato-Doldán, M. H. Rosnes and P. D. C. Dietzel, *ChemSusChem*, 2017, **10**, 1710-1719.
2. P. D. C. Dietzel, V. Besikiotis and R. Blom, *J. Mater. Chem.*, 2009, **19**, 7362-7370.
3. P. Norby, *J. Am. Chem. Soc.*, 1997, **119**, 5215-5221.
4. R. Caliandro, D. Chernyshov, H. Emerich, M. Milanesio, L. Palin, A. Urakawa, W. van Beek and D. Viterbo, *J. Appl. Crystallogr.*, 2012, **45**, 458-470.
5. V. Dyadkin, P. Pattison, V. Dmitriev and D. Chernyshov, *J. Synchrotron Radiat.*, 2016, **23**, 825-829.
6. A. A. Coelho, J. Evans, I. Evans, A. Kern and S. Parsons, *Powder Diffr.*, 2012, **26**, S22-S25.
7. B. H. Toby, *Powder Diffr.*, 2006, 21, 67-70.
8. M. A. García Aranda, A. Cabeza Díaz and A. G. de la Torre in *El método de Rietveld*, (ed. V. J. Esteve Cano) Publicacions de la Universitat Jaume I, 2006, pp. 75.